CLIMATOLOGY

Anthropogenic warming drives earlier wildfire season onset in California

Gavin D. Madakumbura[1,2]*, Max A. Moritz[3,4], Karen A. McKinnon[1,5,6], A. Park Williams[1,2], Stefan Rahimi[1,7], Benjamin Bass[1], Jesse Norris[1], Rong Fu[1], Alex Hall[1,6]

Annual wildfire area in California has rapidly grown in recent decades, with increasingly negative impacts on people. The fire season is also lengthening, with an earlier onset. This trend has been hypothesized to be driven by anthropogenic warming, but it has yet to be quantitatively attributed to climate drivers. Using a comprehensive fire occurrence dataset, we analyze fire season onset and climate controls on its variability and change during 1992–2020 in 13 California ecoregions. Northern California ecoregions show stronger trends toward earlier onset compared to more arid southern California ecoregions. Onset has trended earlier for all but one ecoregion. Interannual variability of onset is dominated by climate variability and its influence on fuel moisture. Trend attribution inferred from onset-climate relationships suggests that anthropogenic warming advanced fire season onset by 6 to 46 days during 1992–2020 in 11 of 13 ecoregions. Continued warming is expected to further promote earlier fire season onsets.

INTRODUCTION

Increasingly large and severe wildfires in the western United States (US) have become more costly in terms of lives lost and damage to property and infrastructure in recent decades (*1*–*3*). In California, wildfire damages in 2018 alone were an estimated $148.5 billion (*4*). Anthropogenic warming has already promoted more fire-conducive conditions across many western US forested areas by increasing surface temperature and evaporative demand (*5*, *6*), and these trends are likely to continue when and where fuels are not limiting (*7*, *8*). In recent decades, a significant positive trend in annual burned area has been observed in forested regions in California, with strong links to the anthropogenic warming in the region (*9*, *10*). A robust understanding of the factors controlling fire season characteristics is vital for comprehending how anthropogenic warming influences fire conditions (*11*, *12*).

Fire season onset timing is a fire season characteristic with practical applications in fire risk outlooks (*13*). An anomalously early onset suggests a potentially longer fire season, with an increased probability of extended burning time and a larger area burned (*14*). Onset has been identified as when fire-weather conditions first surpass a selected threshold (*15*). Some fire-weather indices are heavily influenced by temperature variability and change, and, therefore, defining onset based on these indices may inherently suggest that anthropogenic warming advances onset in many regions (*16*, *17*), including California (*18*). In addition, widely used fire-weather metrics may not represent complex hydrological processes such as snowmelt and snowpack influences on soil moisture (*5*), which influence fuel flammability. While fire-weather is indicative of fire danger, fire occurrence also depends on fuel availability and ignition (*19*). Adding to this complexity is California's high diversity in terms of climate, topography, and ecosystems, which translates to highly diverse fire regimes (*20*, *21*). Therefore, in addition to evaluating the impact of anthropogenic warming on wildfire through the analysis of fire-weather indices, it is crucial to conduct empirical analyses to assess how climate has contributed to variations and trends in the observed fire season onset (*22*). Furthermore, it is essential to disentangle the contributions of anthropogenic warming from those of natural climate variability.

Using records of large fires (defined as fires with a final burned area larger than 400 ha), two previous works have investigated the fire season of the western US. The first study (*23*) highlighted that in high-elevation forests, fires have become more frequent and the wildfire season has lengthened, corresponding with earlier spring snowmelt and increased temperatures. Using the 10th percentile of the start dates of large fires as the fire season onset, the second study (*24*) showed that the onset shifted earlier in higher-elevation and southern ecoregions in the western US during 1984–2011, albeit with nonsignificant trends. Notably, there has been a lack of analyses using fire occurrence records to understand fire season onset. While a correspondence between drying trends and fire season onset has been suggested for a few regions in California in previous work (*23*, *24*), quantifying this effect and extending the analysis to the entire state have yet to be done.

In this study, we investigate changes in fire season onset across the ecoregions in California, using an extensive record of fire occurrence data from 1992 to 2020 (*25*). By analyzing the distribution of recorded fire start dates, we establish a physically interpretable definition of fire season onset. To diagnose the causes of the observed trends in onset, we (i) consider the potential roles of nonclimate factors such as fuel types and ignitions and (ii) provide a detailed decomposition and quantification of climate drivers, distinguishing between natural variability and anthropogenic warming.

RESULTS

Fire season onset

Figure 1 shows the time series of fire season onset (referred to as fire onset from hereon) for the 13 level III ecoregions of California (*26*).

[1]Department of Atmospheric and Oceanic Sciences, University of California—Los Angeles, Los Angeles, CA, USA. [2]Department of Geography, University of California—Los Angeles, Los Angeles, CA, USA. [3]Bren School of Environmental Science and Management, University of California—Santa Barbara, Santa Barbara, CA, USA. [4]University of California Cooperative Extension, Oakland, CA, USA. [5]Department of Statistics and Data Science, University of California—Los Angeles, Los Angeles, CA, USA. [6]Institute of the Environment and Sustainability, University of California—Los Angeles, Los Angeles, CA, USA. [7]Department of Atmospheric Science, University of Wyoming, Laramie, WY, USA.
*Corresponding author. Email: gavindayanga@ucla.edu

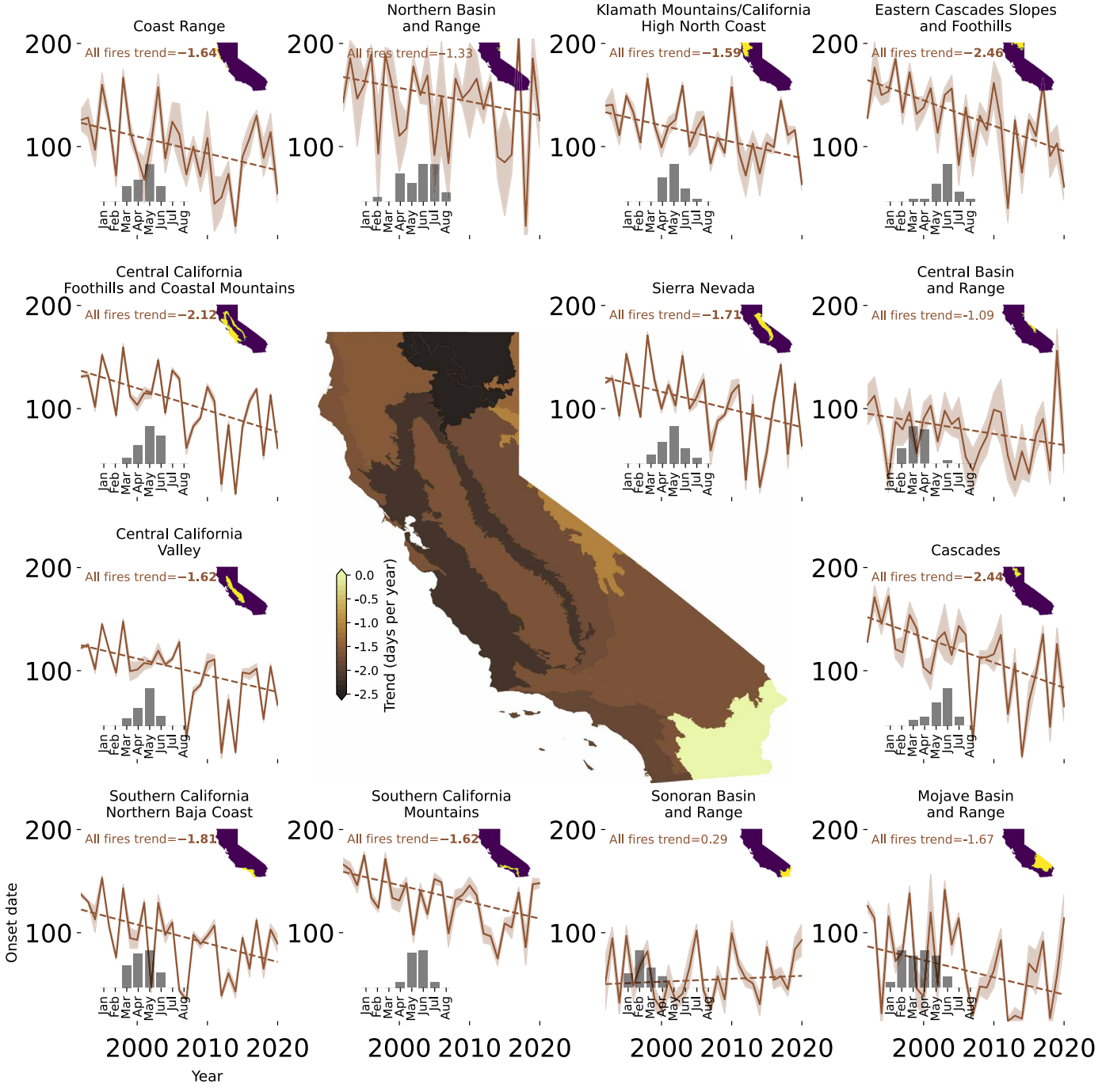

Fig. 1. Trends in fire season onset during 1992–2020. Fire season onset time series (day of the year, shown on *y* axis) for each ecoregion. The subpanel inset histogram shows the distribution of the detrended onset date in months January (Jan) to August (Aug). The best-fit line is shown as a dashed line, with the trend value (days per year) annotated. Regions where $P < 0.05$ are indicated by bold font. False discovery rate of 5% was controlled for *P* values before estimating the significance. *x*-axis ticks are shown for the years 2000, 2010, and 2020 in each subplot. Shading represents the ±1 SD for each year, estimated from 100 bootstrap samples. Best-fit lines are Theil-Sen slopes.

Following (*27*), fire onset is defined as the fifth percentile of the empirical cumulative distribution function of the discovery dates of fires during each calendar year (i.e., the day of the year; fig. S1). Our focus in this study is the main fire season of each ecoregion, which typically peaks in fire occurrence during the summer (fig. S2) when conditions are hot and dry (*21*). We found that the 10th percentile for the Southern California Northern Baja Coast and Sonoran Basin and Range and the 15th percentile for the Southern California Mountains are more suitable for representing the onset of the summer fire season, because of the wind-driven fire season that occurs at the beginning and end of the calendar year in these regions (Supplementary Text). The seasonality of fire onset during 1992–2020

differs across ecoregions (Fig. 1, subpanel insets). Northeastern California (Cascades and Eastern Cascades Slopes and Foothills) shows a peak of fire onset in May to July. By contrast, northwestern and central California (Coast Range, Klamath Mountains/California High North Coast, Central California Foothills and Coastal Mountains, Central California Valley, and Sierra Nevada) have a peak in April to June; in southern California desert ecoregions (Mojave and Sonoran Basins and Ranges), the fire season often begins in the latter part of the cool season (January to March). These contrasts are indicative of the background climates among ecoregions. In addition to a later end to wet season precipitation, northeastern ecoregions have a large snow and subsurface water storage that can carry the moisture from the winter precipitation into spring and summer, delaying fire onset (*28*). Meanwhile, southern California deserts are more arid with an earlier end to a drier wet season, so soil moisture from winter is less persistent through the dry season (*21*). Furthermore, southern California can experience periods of very high fire potential even in winter, as this is the season when high vapor-pressure deficit (VPD) offshore winds (e.g., Santa Ana) are most common and strongest (*29*). Southern California also has extremely high variability in the timing and magnitude of the winter rainy season and precipitation events within it (*30*), likely contributing to the elevated fire onset frequency during multiple months of the year in some ecoregions.

All ecoregions except the Sonoran Basin and Range show a negative trend in fire onset (i.e., fire onset date trends earlier). The arid and semi-arid ecoregions Mojave Basin and Range, Northern Basin and Range, Sonoran Basin and Range, and Central Basin and Range show statistically insignificant ($P > 0.05$) trends. The other ecoregions show significant trends ($P < 0.05$). The most negative trends are observed in the Eastern Cascades Slopes and Foothills (−2.46 days per year), Cascades (−2.44 days per year), Central California Foothills and Coastal Mountains (−2.12 days per year), and Southern California Northern Baja Coast (−1.81 days per year).

Drivers of an earlier fire onset

Fire onset trends toward an earlier fire season can be theoretically driven mainly by three elements that could increase the number of fires and therefore shift or stretch the distribution of fires earlier in the year (fig. S1): (i) increased fuel loads due to, for example, fuel accumulation (*31*), (ii) increased frequency of human-ignited fires, which tend to occur more year-round than lightning-ignited fires (*32*, *33*), and (iii) climate trends such as reduced cool-season precipitation, atmospheric warming, and early snowmelt, which promote the drying of fuels earlier in the year (*23*). We investigate each of these potential drivers to understand their effects.

To investigate the potential influence of fuels, we determine, within each ecoregion, the fire onset for each of the three land cover types where fire is most common (Fig. 2). Changes to fuel loads and other characteristics such as horizontal or vertical continuity can influence the onset if they contribute to a shift in fire occurrence distribution. For instance, increased fuel loads in forests due to fire suppression (*34*) and increased dead and fine fuels from multiyear drought conditions (*35*) can increase the number of fires, and potentially advance onset. Interannual variability of fire onset is highly similar across land cover types within ecoregions (shown as the correlation with fire onset estimated using all fires in Fig. 2). Individual land cover types also follow the trend toward an earlier fire onset in each ecoregion. The largest negative trend in onset among the top three land cover types (Fig. 2, center) is larger than the trend of all fires in the ecoregion (shown in Fig. 1) for 8 of 13 ecoregions. The fraction covered by this land cover type ranges from 16 to 48%. Different vegetation types may have varying sensitivities to the underlying driver responsible for shifting onset earlier in the year. Some fuel types may experience an even stronger shift toward earlier onset than the ecoregion-wide average. In Sonoran Basin and Range, where a trend toward later onset is observed when all land cover types are considered, the shrub land cover type within that ecoregion experienced a trend toward earlier onset (−1.1 days per year; $P > 0.05$). In southern and western ecoregions, developed land is one of the land cover types with the most fire occurrences. A decreasing trend in onset over developed land can be seen in 11 of 13 ecoregions. In the northeast (north of Southern California Mountains and east of Central California Foothills), the land cover type where most fires occur is either tree or shrub, accounting for 47 to 75% of fires in each region. These areas experienced a negative trend in onset, ranging from −0.77 to −1.6 days per year ($P > 0.05$). A few exceptions to the general trend toward earlier onset are observed. In the Sonoran Basin and Range, developed and agricultural lands, which account for 62 and 9% of total fires, respectively, exhibited a nonsignificant ($P > 0.05$) trend toward later fire onset. The tree land cover type in the Central Basin and Range, where 9% of that ecoregion's fires originate, also experienced a nonsignificant trend toward later fire onset. These exceptions aside, the results show a consistent decreasing trend in onset across different land cover types. This suggests that a stronger external driver is influencing the trend toward an earlier fire season and that it is relatively insensitive to the differences in fuel availability and characteristics across land cover types.

The influence of human activities has shaped the distribution of fire occurrences in the US in the recent past (*32*). Natural ignitions through lightning tend to be limited geographically to high elevations and follow a seasonal cycle (*36*). Human ignitions generally cause the fire season across California to be broader than it would be with lightning ignitions alone (*32*, *37*, *38*). Human ignitions are inherently compound events, driven by both the number of accidental or deliberate ignitions and the environmental conditions (climate and fuel) that allow a fire to ignite. However, it is hypothesized that the human ignition potential has increased over time because of rising human activities (*32*, *38*). Increasing human ignitions can shift or stretch the distribution of fire occurrences, making the fire onset earlier. However, the annual frequency of human-ignited fires actually significantly declined during our study period (Fig. 3). In the month that represents the most common fire season onset, the trend in the frequency of human ignitions was either zero or negative for 11 of 13 ecoregions. Larger negative trends in human-ignited fire counts are observed later in the fire season, wherein the total number of fires is generally higher (fig. S2). These trends suggest that changes in human ignition frequencies do not contribute to an earlier onset. All else equal, reductions in human ignitions may promote a narrowing of the fire count distribution and a later onset, given that nonhuman ignitions are most common in the summer (*32*).

Climate variability can influence the timing of the fire season by altering interannual variations in hydrological processes, which, in turn, change fuel moisture levels. Anthropogenic warming can make the fire onset earlier primarily by shifting the temperature distribution toward warmer values, leading to warmer winter and spring temperatures, earlier snowmelt, enhanced evaporative demand, and,

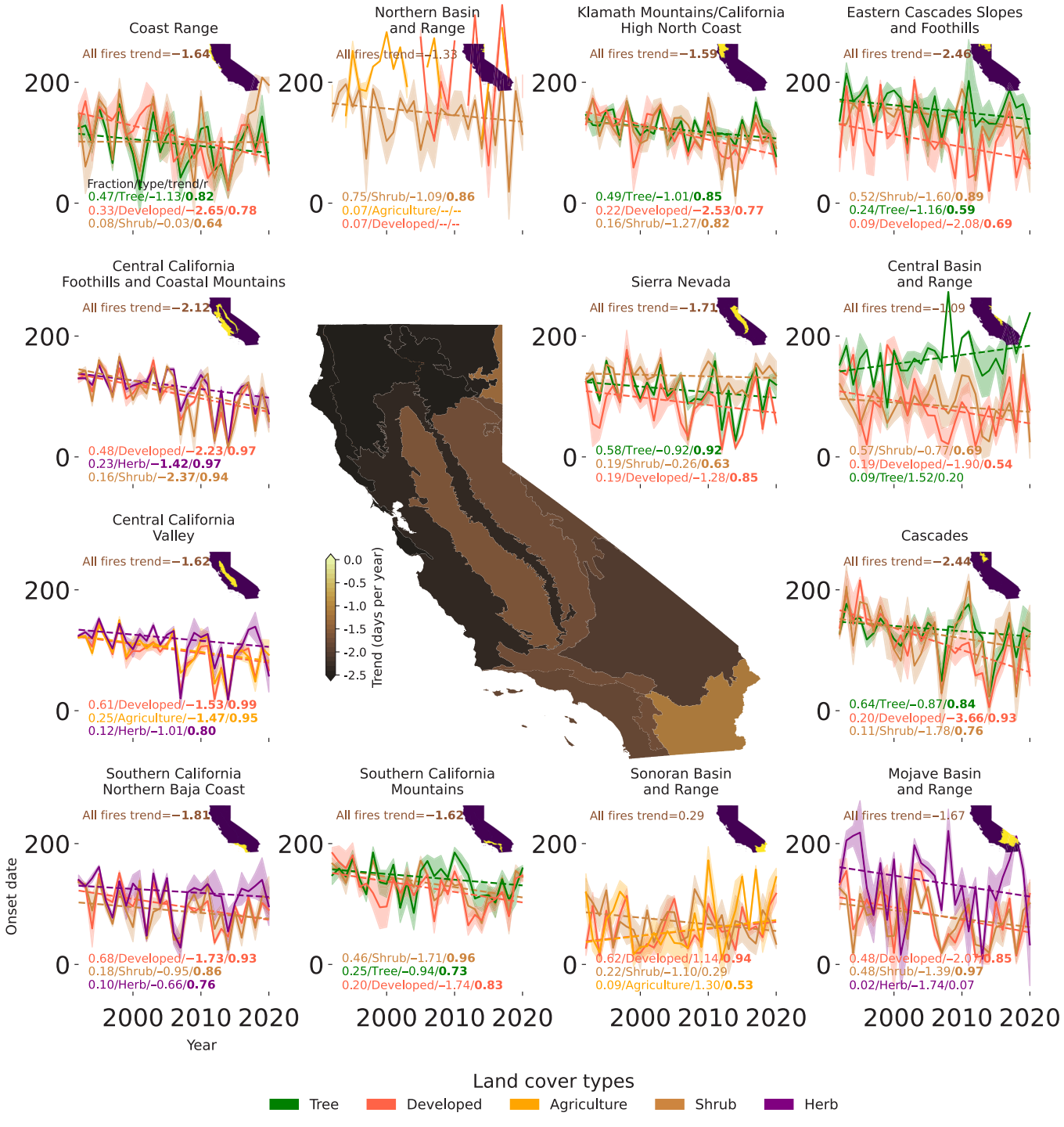

Fig. 2. Trends in fire season onset during 1992–2020 for different land cover types. Fire season onset time series (day of the year, shown on *y* axis). Green, red, orange, brown, and purple colors are used for Tree, Developed, Agriculture, Shrub, and Herb, respectively. Results for land cover types that contain the three highest numbers of fires in each ecoregion are shown. For different land cover types, the fraction of fires during the period is annotated, along with the land cover type name, the linear trend of fire onset in days per year, and the correlation with the fire onset derived from all fires, respectively. Dashed lines show the best-fit line. The spatial map of California in the middle shows the largest negative trend among the three time series for top land cover types and the time series for all fires for each ecoregion. The trend for the entire ecoregion is annotated above the time series in each panel. Statistically significant trends and correlations ($P < 0.05$) are indicated by bold font. False discovery rate of 5% was controlled for before estimating the significance. Shading represents the ±1 SD for each year, estimated from 100 bootstrap samples. Best-fit lines are Theil-Sen slopes.

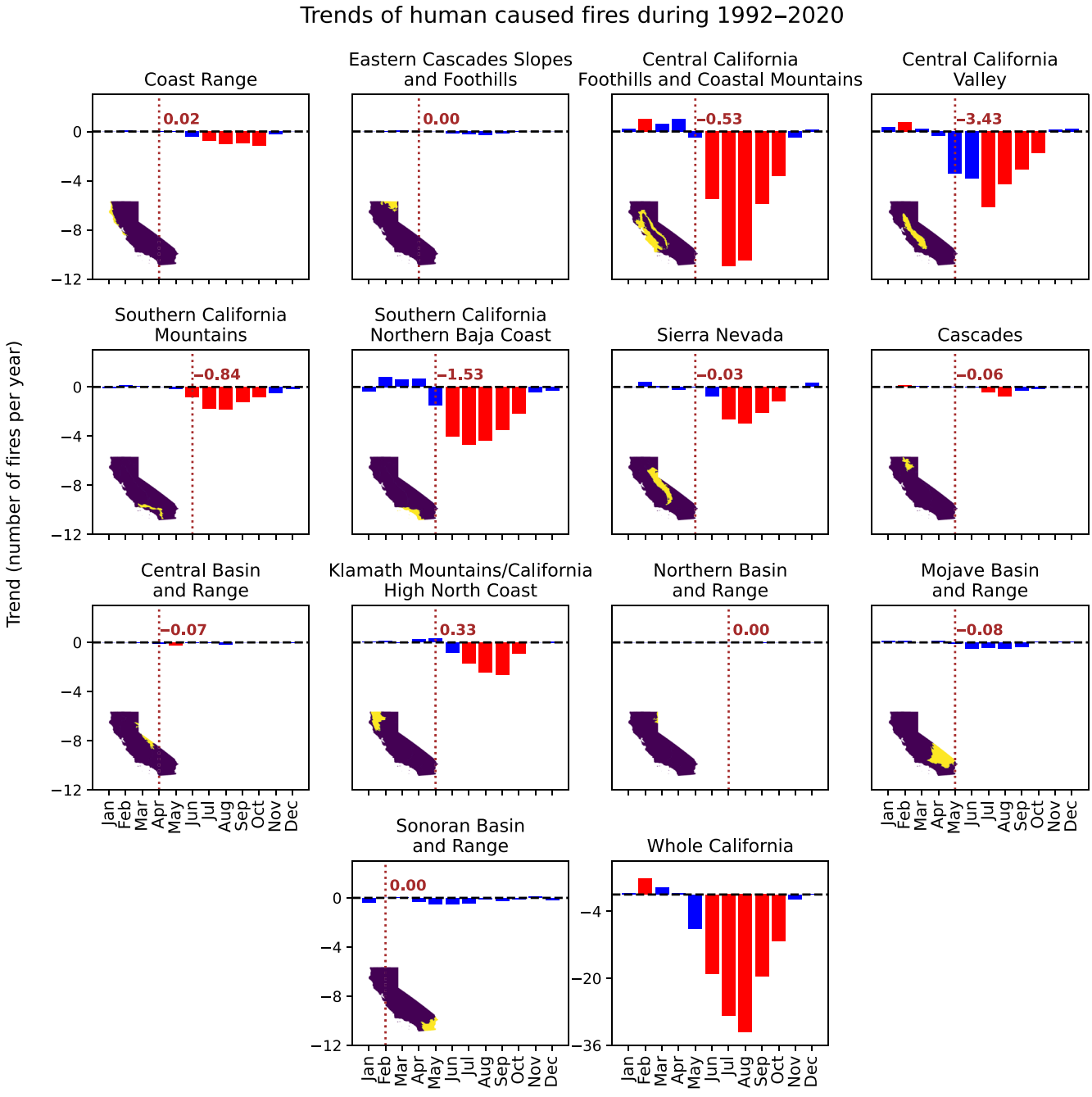

Fig. 3. Trends in the number of human-caused fires during 1992–2020. Statistically significant ($P < 0.05$) trends are shown in red. Note that the *y* axis range is different for the bottom-right panel, which represents data for the entire state of California. Dashed vertical line represents the mode of the monthly distribution of onset during the study period. Trend value corresponds to the mode of onset is annotated. False discovery rate of 5% was controlled for before estimating the significance.

consequently, drier fuels. To investigate the influence of climate, we show the correlation between the detrended fire onset and detrended climate time series of different seasons in Fig. 4 and fig. S3. Cool-season (December to March) soil moisture is generally the variable with the highest correlation and is statistically significant for all but three ecoregions. This correlation is greatest for the Southern California Mountains (0.92), Central California Foothills and Coastal Mountains (0.89), Sierra Nevada (0.87), Sonoran Basin and Range (0.83), and Southern California Northern Baja Coast (0.82). Winter precipitation generally has the next highest correlation, although this likely reflects mostly the same information as soil moisture. Spring to summer VPD shows strong negative correlations (fig. S3), especially for the Southern California Mountains (−0.77), Klamath Mountains/California High North Coast (−0.75), and Sierra Nevada (−0.71). This is similarly reflected by strong negative correlations with temperature in the same months. In high mountainous regions

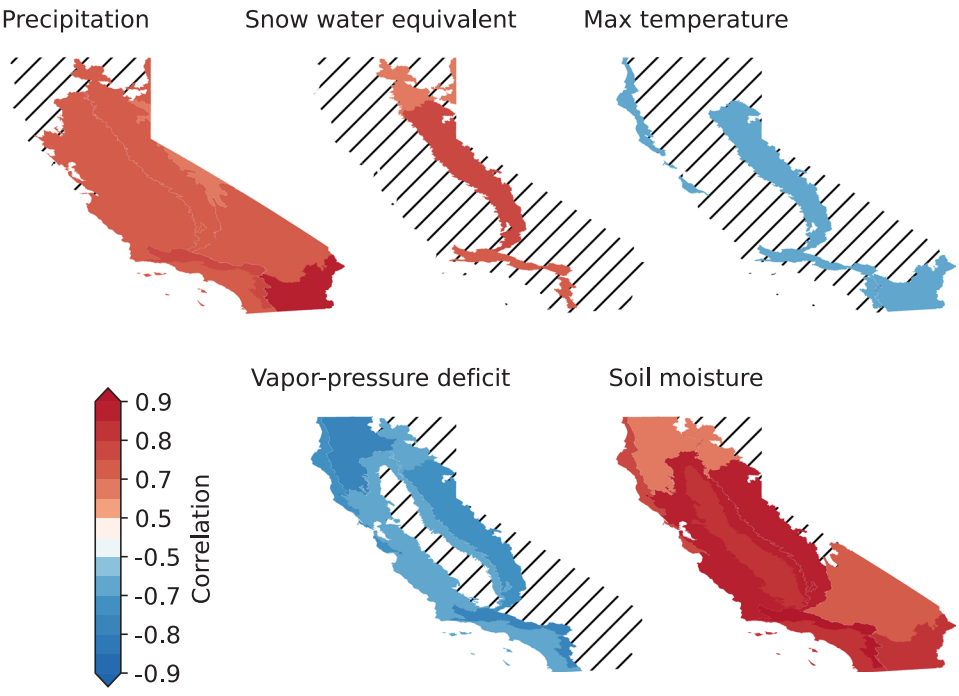

Fig. 4. Relationship between climate variables and fire season onset. Correlation between detrended fire season onset and detrended precipitation, snow water equivalent, maximum temperature, VPD, and soil moisture. Correlation is calculated against the given variable, averaged over each antecedent 3-month running period (DJF, JFM, etc.). Lag values are considered from December of the previous year up to fire season onset. The strongest correlation for each variable across all seasons is shown here. Only regions where the correlation is significant ($P < 0.01$) are shown, and regions where correlation is not statistically significant are marked with hatching. False discovery rate of 1% was controlled for before estimating the significance.

(Sierra Nevada, Southern California Mountains, and Cascades), onset date correlates positively with snow-water equivalent (0.77, 0.72, and 0.67, respectively), indicating later onset with heavier snowpacks. It should be noted that fire season onset is derived solely from fire occurrence data and is, therefore, completely independent of the climate data in terms of data generation. The very strong correlations observed are thus indicative of the dominant climate control over onset variability. Overall, these relationships indicate that winter precipitation and snow can influence the fire onset through delayed effects on soil moisture and VPD, while spring to summer temperature and VPD can influence fire onset over shorter timescales.

Relationship between fuel moisture and fire season onset

To further investigate how climate can influence fire onset, we examine the relationship between fire onset and fuel moisture. Remote sensing–based estimates of vegetation moisture content can provide more spatially and temporally complete data compared to direct measurements of live fuel moisture content (LFMC) (*39*). Remote sensing–based reconstructions of dry-season (July to August) canopy water content (CWC) of vegetation canopy above 2 m in height (*40*) show significant positive correlations with fire onset across California (Fig. 5A). This strong relationship is particularly evident in southern California ecoregions, Central California Foothills and Coastal Mountains, Cascades, and the southern Sierra Nevada. We also investigate the potential role of fuel moisture using direct measurements of LFMC from the National Fuel Moisture Database for regions with continuous temporal coverage (see Materials and Methods). Fire onset is significantly correlated with direct measurements of LFMC (Fig. 5, B to E), in particular for the Central California Foothills and Coastal Mountains ($r = 0.69$), Southern California Mountains ($r = 0.71$), Southern California Northern Baja Coast ($r = 0.77$), and Sierra Nevada ($r = 0.66$). Regions with particularly high fuel moisture and fire onset correlation in Fig. 5 also stand out as the regions where the soil moisture–onset correlations in Fig. 4 are strong. These results indicate that fuel moisture is the dominant driver of interannual variability in fire onset date throughout much of California, with interannual variability in fuel moisture being driven by fluctuations in precipitation supply and evaporative demand (*40*, *41*). These results provide additional evidence of the onset-climate relationship through an independently derived measure.

Roles of natural variability and anthropogenic warming on observed fire season onset trends

We next decompose the influences of climate drivers on the observed fire onset trend. Using a causal effect network (CEN) framework (*42*–*44*), we identify the climate variables and seasons most likely to have a causal influence on fire onset for each region (see Materials and Methods and fig. S16). Precipitation during the early months of the wet season (October of the previous year to February of the current year) is a dominant causal variable for onset across most ecoregions. Precipitation from late winter through spring is particularly important for some arid and desert ecoregions, such as the Mojave Basin and Range, Southern California Mountains, and Central Basin and Range. The effect of current-year VPD is evident in many ecoregions, particularly the Sierra Nevada, Southern California Mountains, and Cascades ecoregions, which also exhibit a significant correlation between snowpack and fire onset (Fig. 4). We model the fire onset of each ecoregion as a linear function of causal climate

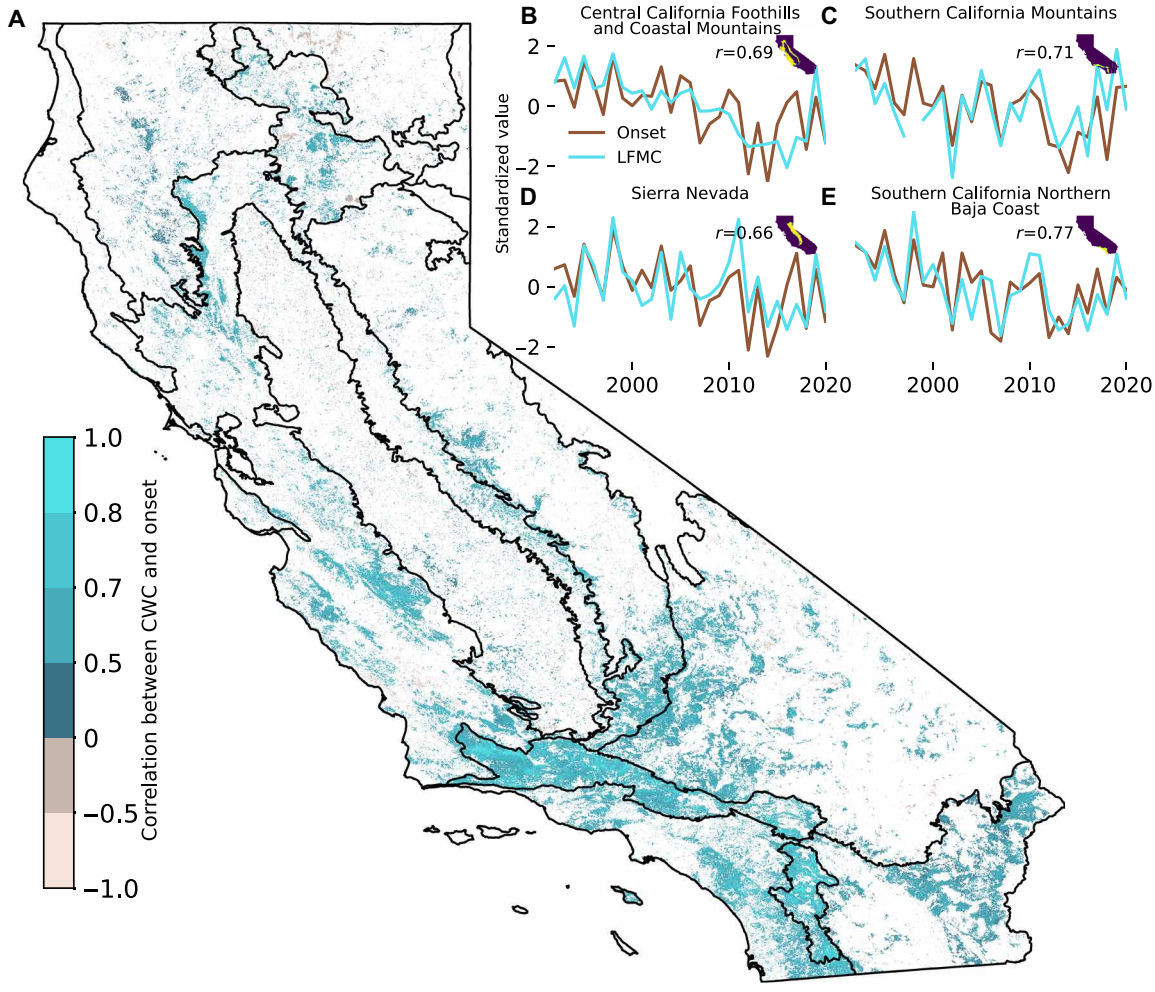

Fig. 5. Relationship between fire season onset and measures of vegetation moisture. (**A**) Correlation between fire season onset and reconstructed CWC using remote sensing and environmental data for the period 1992–2017. Each grid cell value represents the correlation between that grid cell's canopy water record and the fire onset record for the ecoregion that the grid cell lies within. (**B** to **E**) Time series of the fire onset and representative LFMC measurements during 1992–2020 for Central California Foothills and Coastal Mountains (B), Southern California Mountains (C), Sierra Nevada (D), and Southern California Northern Baja Coast (E). Correlation between fire onset and LFMC (*r*) is shown in (B) to (E). Only statistically significant values, after controlling for a false discovery rate of 20% (with a corresponding *P* value of 0.04) are shown in (A).

variables (table S1). Next, the time series of each climate variable is separated into natural variability and thermodynamic components using the dynamical adjustment technique (Materials and Methods). In brief, dynamical adjustment isolates the variability of the target climate variable that is linked to the variability in atmospheric circulation (*45*–*48*). This is the dynamical component, which is interpreted as dominated by natural variability. The residual contains the thermodynamic change, interpreted as dominated by anthropogenic warming. Using these time series of natural variability and anthropogenic warming components, the contribution of each component to the fire onset trend is estimated (Fig. 6 and fig. S4).

We estimate that natural climate variability contributed to a large negative trend in fire onset date (toward earlier) for most ecoregions during our 1992–2020 study period. California experienced a severe multiyear drought during 2012–2015 (*49*, *50*), which was a major factor driving this natural variability component. The largest contribution from natural variability can be seen in the arid/semi-arid regions of the Mojave Basin and Range [accounting for a trend of −28 ± 22 days (means ± 1 SD), from 1992 to 2020] and the Southern California Mountains (−22 ± 16 days). The smallest influence of natural variability is observed in the Sonoran Basin and Range (−5 ± 13 days).

Central estimates of distributions show that anthropogenic warming contributed to an earlier fire onset in 11 of 13 ecoregions. This is particularly pronounced in the Cascades (−46 ± 9 days), Northern Basin and Range (−31 ± 9 days), and Sierra Nevada (−24 ± 7 days). Meanwhile, in southern California desert ecoregions, anthropogenic warming contributed to a slight delay in fire onset, ranging from +7 ± 8 days in the Mojave Basin and Range to +14 ± 9 days in the Sonoran Basin and Range. One possible reason for this is that these regions are more fuel limited, where moisture is needed for fuel growth, making the climate-onset relationship more complicated (*51*, *52*). Another possible reason is that anthropogenic warming strongly affects temperature but may affect precipitation in more nuanced ways, for example, by intensifying precipitation events (*53*). In regions where precipitation totals and timing have a

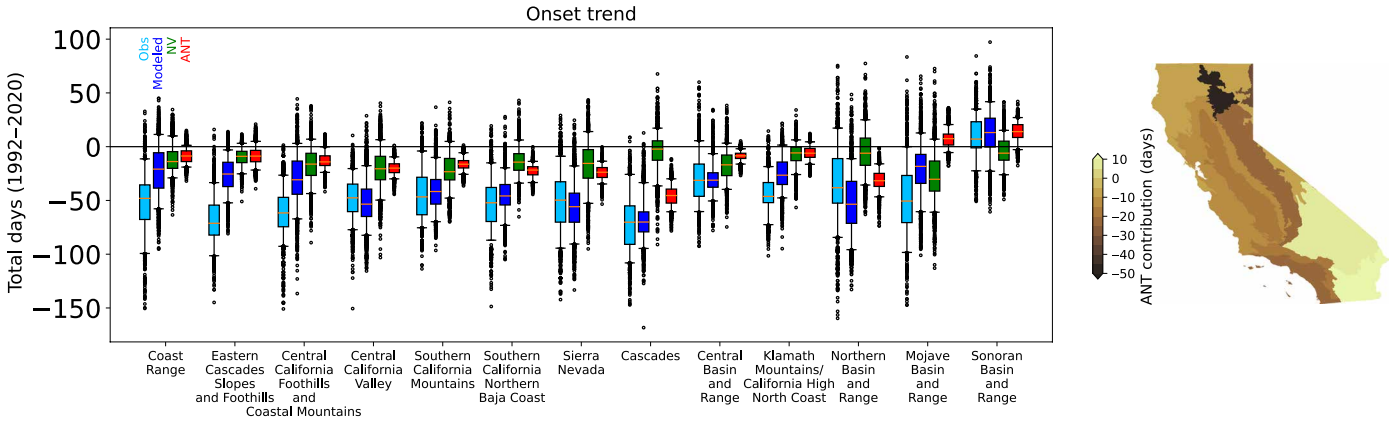

Fig. 6. Influence of natural variability and anthropogenic warming on observed trend in fire season onset. Trends in observed fire season onset from 1992–2020 (Obs, light blue) and fire onset modeled using total climate variability and trend (Modeled, dark blue), natural variability (NV, green), and anthropogenic warming component of climate variables (ANT, red). Modeled trend distributions are created by considering the uncertainty of the regression model and trend estimation, yielding 2900 values per region (Materials and Methods). The uncertainty of the observed trend is estimated using leave-one-out sampling. Box plots indicate the median (orange horizontal line) and the interquartile range. Whiskers show the 2.5th and 97.5th percentiles. Outliers are shown by circles. Right panel shows the mean ANT contribution for each region.

stronger effect on fire onset, such as southern California (Fig. 4 and fig. S3), the impact of anthropogenic warming is expected to be weaker.

Climate variables do not fully account for the observed trends in fire onset in some ecoregions (as indicated by the difference between observed and modeled trend distributions in Fig. 6). Particularly in the Coast Range, Eastern Cascades Slopes and Foothills, and Central California Foothills and Coastal Mountains, the linear model for onset explains only 51, 30, and 59% of the variability, respectively. Possible reasons could include nonlinear climate influences not captured by our linear models or other factors not accounted for in the modeling framework.

DISCUSSION

Understanding how anthropogenic warming influences fire onset is critical for assessing the increased probability of fire occurrence. Previous efforts to understand fire onset have generally focused on the onset of fire-weather, but not the actual onset of the fire season (*15*, *54*). Fire-weather indices are largely indicative of the atmospheric evaporative demand and near-surface soil moisture and, therefore, serve as proxies for fuel moisture. However, they do not consider fuel load, fail to capture complex ecohydrological processes and feedbacks, and do not fully represent mechanisms relevant to fire onset (*55*). Our results based on fire occurrence data present an estimate of fire onset that is physically consistent with variations in surface and subsurface water budgets and fuel moisture across the distinct climate regimes of California.

Our results highlight a geographical divide across California in the contributions of anthropogenic warming versus internal variability to fire onset trends. A large, fire onset–promoting influence of anthropogenic warming in northern California ecoregions (e.g., Cascades, Sierra Nevada, and Northern Basin and Range) stems from the strong influence of temperature, likely by accelerating snowmelt (*23*, *28*) and evapotranspiration (*56*). Anthropogenic warming in California has already emerged from the interannual temperature variability (*57*). This indicates a continuing shift in the distribution of fire onset in northern California beyond the envelope of natural variability.

There is a large natural variability in precipitation in California (*58*), and considerable uncertainty remains regarding whether anthropogenic warming is increasing or decreasing precipitation (*59*). This makes the detection and separation of the anthropogenic warming component of precipitation challenging (*60*) and implies a large uncertainty in the estimates of the anthropogenic warming contribution. More subtle changes in precipitation characteristics, such as a shortening of the wet season (*61*), a decrease in precipitation frequency (*55*, *62*), and an increase in the amount of water vapor available for intense precipitation events (*53*), could also influence statistics of aggregate fire season characteristics, such as fire onset. Anthropogenic warming also alters the precipitation partitioning in California, shifting from snow-dominant to rain-dominant (*63*), thus modifying the fire-climate relationships identified in this study. In future work, climate-based modeling of fire onset presented in this study could be modified to incorporate these nonlinear changes in precipitation characteristics.

The climate control of fire onset is ubiquitous across California, in ecoregions with varying vegetation characteristics, from deserts to forests. The assessment of fire onset aggregated across an ecoregion may give more weight to the more fuel-abundant areas within the ecoregion. Other fuel characteristics can also exhibit interannual variability (*64*). For example, wet years can promote fuel growth in fuel-limited regions (*51*, *52*); meanwhile, drought may lead to vegetation mortality, which may further increase fire risk beyond that expected from fuel drying alone (*35*). However, we found similar trends in fire onset across different vegetation types. Future analysis can evaluate the role of land cover in modulating the effect of fuel moisture on fire onset.

Climate variability shapes fuel availability, ignition efficiency, and fuel combustibility, irrespective of the ignition sources (*65*, *66*). However, most fire ignitions in California are caused by human activities, which have major impacts on the number and seasonality of wildfires in the state, particularly by widening the fire season beyond the summer months when lightning is most common (*32*, *37*).

Therefore, we expect that the observed decrease in human-ignited fires (Fig. 3) (*37*) would, all else equal, promote a delayed fire onset. Last, the differences in fire onset variability and trend in different land cover types (Fig. 2) could be partly due to the limitation of human ignition, especially in regions far from human population and activities (*38*).

Our analysis provides a framework for understanding the mechanisms through which climate controls fire onset. The anthropogenic warming component in predicting fire onset is indicative of what is to come, as warming trends continue. Thus, our findings have major implications for wildfire seasonal predictions and disaster prevention and management strategies in coming seasons and years.

MATERIALS AND METHODS

Fire occurrence and climate data

We use the sixth edition of the US Forest Service Fire Program Analysis–Fire Occurrence Database (FPA-FOD) (*25*). The dataset is quality controlled and comprehensive and includes ~2.3 million wildfires recorded by US federal, state, and local agencies during 1992–2020. In our analysis, we use the data attributes discovery date, location (latitude and longitude), and ignition cause classification (human-caused or natural).

To investigate the climate drivers of fire season onset, we obtained observed monthly precipitation, snow water equivalent, maximum and minimum temperature, VPD, and soil moisture from TerraClimate (*67*), which has a 1/24th degree spatial resolution for the period 1960–2020. For dynamical adjustment to isolate the natural variability, we use ERA5 (*68*) sea level pressure (SLP) data for the period 1960–2020.

Considering the spatial heterogeneity of climatic conditions and fire season characteristics (*21*) within California, we analyze 13 ecoregions based on the US Environmental Protection Agency's ecoregion level III classification (*26*). These ecoregions represent vegetation characteristics and climate conditions, from deserts to forests, and, therefore, results can implicitly indicate the role of vegetation in the onset-climate relationship.

Live fuel moisture data

We use dry-season (July to August) liquid water in canopy above 2 m in height, created using deep learning for 1992–2017 (*40*). This dataset (*69*) has been developed using remotely sensed canopy water estimates and environmental data (e.g., elevation, slope, aspect, relative elevation, LANDSAT 8 surface reflectance, distance to the nearest road, road density, maximum incident solar irradiation from four periods throughout the year, and spatial coordinates). More specifically, (*40*) used high-fidelity imaging spectroscopy and light detection and ranging data collected during August 2015, July 2016, and August 2017. Using these remote sensing data, CWC was estimated for a total of 2.09 million ha of nonoverlapping coverage. A fully connected neural network with four hidden layers with 200 neurons each was trained to model the estimated CWC using above environmental data. The year 2012 is missing from this dataset due to missing LANDSAT training data. More details on the deep learning model can be found in (*40*). Original data of CWC at 30-m spatial resolution is regridded to a 270-m grid (*70*) for the analysis.

While remotely sensed CWC can serve as a proxy for live fuel moisture, it may not fully represent direct measurements of fuel moisture. As an independent measurement of fuel moisture, we use directly measured LFMC from the National Fuel Moisture Database. LFMC is the ratio of the mass of water contained in a live plant to its total dry mass. We first select sites across California with at least one LFMC measurement during the August to September period and at least 25 years of summer data from the 1992–2020 study period. Recognizing the potential impact of data gaps, particularly during extreme climatic events such as multiyear droughts or wet periods, we refine the selected dataset by excluding sites with any 3-year consecutive period of missing data, aiming to mitigate distortion in our correlation calculations. This provides at least one site for ecoregions Central California Foothills and Coastal Mountains, Southern California Mountains, Southern California Northern Baja Coast, and Sierra Nevada. We combine the regions with multiple sites to obtain one representative time series for each region.

Land cover data

To investigate fire onset across different land cover types, we use annual land cover data from the National Land Cover Database (*71*). We consolidate land cover classes into broader categories: Developed (all intensity levels of developed land), Tree (deciduous, evergreen, and mixed forest types), Shrub (shrub, scrub, and dwarf scrub), Herb (grassland/herbaceous and sedge/herbaceous), Agriculture (pasture/hay and cultivated crops), Wetlands (woody wetlands and emergent herbaceous wetlands), Barren (barren land rock/sand/clay), Water (open water), and Snow-Ice (perennial ice/snow). For each fire event, the land cover type of the year of the fire is selected based on the latitude and longitude data recorded for the fire.

Estimation of causal climate drivers

To estimate the influence of natural variability and anthropogenic warming, we first develop a CEN following (*42*). We aim to model the onset based on climate and meteorological conditions. We choose multiple linear regression because its results and coefficients are easily interpretable. To select causal drivers for the regression model, we use the CEN, which applies the PCMCI causal discovery algorithm (*43*, *44*). The PCMCI combines the PC algorithm (named after Peter Spirtes and Clark Glymour) (*72*) with momentary conditional independence (MCI) to adapt it for time series data. The process consists of a conditioning-selection step (PC) followed by the MCI step. If one aims to identify the causal link between X and Y (where X and Y are assumed to be the independent and dependent variables, respectively), the causal discovery algorithm can detect causal relationships while overcoming challenges such as the autocorrelation of X, an indirect effect of X on Y via a third variable, or the presence of a common driver influencing both X and Y. Details about the PCMCI algorithm are provided in (*43*, *44*), and (*42*) presents a step-by-step example of its application to Arctic teleconnection pathways, which we follow here. The methodology is outlined below with an example from the Southern California Mountains ecoregion (figs. S8 to S15).

The algorithm consists of a causal discovery phase, during which the causal network is identified for a target variable. The starting point is a fully connected graph, as shown in fig. S8 for the Southern California Mountains. Applying this algorithm to onset requires adaptation. Onset is annual, whereas climate time series are on a monthly scale. In addition, onset timing varies by region (Fig. 1). To account for this, we define the latest month of onset in the historical record as the starting month ($t = 0$) and look back up to a selected lag (in this example, up to $t - 18$). Specifically, we consider lags

extending to December of the previous year to capture the preceding wet season, making the total lag 18 months in this example. We consider the following as key drivers of fire onset: seasonal average precipitation, maximum and minimum temperatures, and VPD. Effects of antecedent conditions, such as rainfall and snowfall, and temperature persist into later seasons via soil moisture and, therefore, fuel moisture, thereby influencing the fire onset. Furthermore, antecedent climate conditions can influence the fire season by increasing fuel load in fuel-limited regions. This is in addition to the concurrent meteorological conditions, such as VPD, which can influence fire onset through influencing dead/fine fuel moisture (*51*, *52*). For example, in regions where the fire season window (gray shaded area in fig. S3) ends in June-July-August (JJA), we analyze the aforementioned variables across seasons: December-January-February (DJF), January-February-March (JFM), February-March-April (FMA), March-April-May (MAM), April-May-June (AMJ), May-June-July (MJJ), and JJA of the current year, as well as DJF to November-December-January (NDJ) of the preceding year. This results in 19 seasonal time series for each variable, yielding a total of 76 potential predictor time series (19 seasonal time series for each of the four variables). The CEN framework provides a methodology based on causal discovery to identify the most important variables from this initial list. It should be noted that, since the relationship between meteorological conditions and onset is assumed to be mediated through soil and fuel moisture, we use 3-month mean conditions rather than monthly values. This is because soil moisture is an integrated climate variable that depends on antecedent conditions.

After setting up the initial fully connected graph, the edges between the target variable (onset) and other variables at a given time lag are tested for removal using conditional independence tests. In this analysis, we use partial correlation, following (*42*). As the first step, we calculate the correlation between the fire onset time series of each year and antecedent climate variables (e.g., fig. S3) and select cases where the correlation is statistically significant at a P value threshold of α ($P < \alpha$). In this example, α is set to 0.05. This set of selected variables is referred to as potential parents (Po). For the Southern California Mountains, the Po variables, along with their correlation coefficients (r values) and P values, are shown in fig. S9. Next, the Po variables are sorted based on the absolute value of their correlation with fire onset. Conditional independence tests are then performed between each Po variable and fire onset, starting by removing the influence of the variable with the highest correlation (denoted as Z). This is done by calculating the partial correlation. In the given example, ppt_JFM is selected as Z. If a variable X has a statistically significant partial correlation with fire onset, it is considered to have an independent influence on fire onset beyond Z. Conversely, if the partial correlation is not significant, X is removed from further analysis. In this case, we assume that there is no direct influence from X and onset and that the observed significant correlation between X and onset is due to the indirect influence through Z (*42*). The causal principle that a variable must precede in time or occur simultaneously with another variable to influence it is always enforced as a time-order constraint.

In the given example, conditioning on ppt_JFM removes the following variables from the parent list (Po): ppt_MJJ, tmax_JFM, tmax_FMA, tmin_MAM, tmin_AMJ, tmin_MJJ, tmin_JJA, vpd_JFM, and vpd_FMA (fig. S10). This process objectively refines the Po list into a smaller subset (P1). The process is then repeated by conditioning on the next variable in P1 with the highest absolute correlation with fire onset. This step is illustrated in figs. S11 to S14 using additional variables from Po. After evaluating conditional independence for a single variable, we incrementally include two, three, and more variables (e.g., fig. S15), continuing until the final list of independent variables converges. Last, we develop an ordinary least squares (OLS) regression model for fire onset in each ecoregion, using the selected climate drivers (table S1). With these identified drivers and onset models, we then quantify their influence on fire onset (Fig. 6 and fig. S4). The final list of variables for the example case includes ppt_FMA, ppt_DJF, ppt_lag1_NDJ, and tmin_lag1_SON. Notably, ppt_DJF and ppt_lag1_NDJ share common months (December of the previous year and January of the current year). However, the causal discovery algorithm identifies these two variables as having unique, independent influences on onset, despite their shared temporal overlap (figs. S12 and S13).

To estimate the robustness of the causal discovery results, we use a moving block bootstrap approach (*73*). We generate 1000 block-bootstrapped samples using a block size of 3 years. In this method, each block consists of 3 consecutive years, and resampling is performed with replacement at the block level. The selected blocks may overlap, ensuring that temporal dependencies within each block are preserved while allowing for variability in the resampled dataset. Figure S16 shows the top 10 variables for each ecoregion, ranked by the percentage of selection as causal drivers. The causal drivers identified from the full time series (table S1) remain the dominant variables in the bootstrapped results (fig. S16). For instance, in the Southern California Mountains, the causal variables obtained from the full time series are the top four most frequently selected across the 1000 resamples. The FPA-FOD dataset has a large number of very small fires (*74*). We redid the above bootstrap analysis by removing fires smaller than 0.4 ha (1 acre), which removes 59% of all fires in the dataset (*74*). While this limits the information through limiting the sample size, we largely find similar causal drivers for many of the regions (fig. S17).

The significance level α, chosen for the causal discovery algorithm, can have a notable impact on the results. To assess this sensitivity, we repeated the above steps for α values of 0.01, 0.05, 0.1, and 0.2 (table S2). For lower α levels, the variables most frequently identified in the moving block bootstrap resampling results (fig. S16) are the ones predominantly selected by the causal discovery algorithm. Increasing α allows for more flexibility, enabling the inclusion of additional variables. These are also among the top causal drivers appearing in the bootstrapped results. On the basis of this assessment, we retain results from $\alpha = 0.05$ for the next step. In addition, the correlation between onset and a given variable can be either positive or negative, reflecting the fact that California consists of both water- and energy-limited regions. Therefore, all correlation tests are two-tailed, effectively reducing the α level by half (e.g., for $\alpha = 0.05$, the actual threshold for significance is 0.025, and so on).

The resulting OLS regression model for onset, using the identified causal drivers as independent variables, is presented in tables S1 and S3. All models are statistically significant [Prob(F) < 0.05], residuals appear to be normally distributed based on the Omnibus test [Prob(Omnibus) > 0.05], no strong autocorrelation is detected based on Durbin-Watson (between 1.5 and 2.5), and no strong multicollinearity is observed based on the condition number (<6) (table S3).

The causal discovery approach relies on several key assumptions and has inherent limitations. One is the Causal Markov Condition,

which implies that the parents (final causal drivers) of the target variable form a sufficient conditioning set to establish conditional independence with any other variable. Another is Causal Sufficiency, which assumes that all common drivers of the target variable are included among the observed variables. In addition, the Faithfulness Assumption indicates that the conditional independencies observed in the data arise from the structure of the causal graph itself. Beyond the uncertainties introduced by these assumptions, causal discovery results can also be influenced by data nonstationarities, nonlinear relationships between variables, and the choice of conditional independence tests. We used Pearson correlation during the causal discovery step in this study, assuming a linear relationship between variables. However, using Spearman rank correlation yielded largely similar causal drivers for onset (fig. S18), indicating that the linearity assumption was broadly satisfied. While nonlinear conditional independence tests that are nonparametric and can generalize for nonlinear relationships are available, they may struggle to identify true causal relationships when the sample sizes are smaller, such as in this study (number of years = 29) (*43*). Moreover, while we demonstrate the sensitivity of results to the chosen significance level, an important next step is to implement false discovery rate control to ensure the robustness of causal inferences (*43*). A comprehensive discussion of the assumptions, data constraints, and methodological challenges in causal discovery can be found in (*43*, *44*).

Estimation of the influence of natural variability and anthropogenic warming

To isolate the influence from natural climate variability, we use the dynamical adjustment technique (*45*–*48*). Dynamical adjustment isolates the variability of the target climate variable that is linked to the circulation-induced variability. This is the dynamical component, which we treat as an estimate of natural climate variability. The residual contains the thermodynamic change. Dynamical adjustment assumes that external forcings from anthropogenic emissions exert a thermodynamic response in $y0$, which is distinct from the random internal variability that influences $y0$ through circulation anomalies. Therefore, the residual of the model of $y0$, using a proxy for circulation, is assumed to be a noise-filtered estimate of the thermodynamic response of $y0$ to external forcing. We then approximate the anthropogenic warming as the trend in the thermodynamic response (*48*). Following (*47*), we use the SLP of the domain Northern Hemisphere 0°N to 80°N Pacific/North America sector 110°E to 290°E as the variable that represents the circulation change and use partial least squares (PLS) regression to map a target climate variable for a given season of all ecoregions (dependent variable, $y0$) onto the SLP (independent variable, $X0$). We first remove the low frequency variability of $X0$ ($X_{\text{low\_freq}}$) and $y0$ ($y_{\text{low\_freq}}$) using nonparametric locally weighted scatterplot smoothing. This approach accounts for the forced response in circulation, assuming that the forced change in circulation is sufficiently smooth (*45*, *48*). Then, the $y = y0 - y_{\text{low\_freq}}$ is mapped onto the $X = X0 - X_{\text{low\_freq}}$ using PLS regression. The number of PLS components was selected using leave-one-out cross-validation. Natural variability component (dynamical component) is then estimated as the PLS modeled estimate (y_{mod}) and the thermodynamic component is taken as the residual, $y0 - y_{\text{mod}}$. We follow this procedure for each variable and each season, separately. Once we separate the natural variability and thermodynamic component of each climate driver used to model fire onset, the contribution from each component on the fire onset trend is estimated.

SLP is used to represent circulation, as opposed to other circulation proxies such as geopotential height, since the latter may be more influenced by surface temperature fields (*45*). In addition, SLP of the selected domain has been successfully applied in dynamical adjustment for this target domain in previous studies (*46*, *47*). It is important to note that the dynamical adjustment technique is just one among several methods available for this task (*75*). The impact of methodological uncertainty on the quantitative estimates provided may warrant further studies.

Uncertainty estimation of the regression model

The uncertainty in regression coefficients is calculated by applying a leave-one-out procedure. For each sample, we remove 1 year at a time and recreate the climate-onset least squares regression model, resulting in 29 different models.

For the uncertainty in the trend estimates and soil moisture contribution to fire onset (total, natural variability, and anthropogenic warming), we randomly resample the years with replacement and calculate the trend of observed fire onset, modeled fire onset, natural variability component, and anthropogenic warming component, for 100 samples. To estimate the uncertainty of the attribution of observed trends in fire onset to trends in modeled, natural variability and anthropogenic warming, we calculate the contribution of trends for each of the above-created 29 leave-one-out regression models. This results in 2900 estimates for each variable.

All trend estimates in this study are calculated using the nonparametric Theil-Sen estimator (*76*, *77*), and the P values are estimated using the Mann-Kendall trend test (*78*, *79*). False discovery rate is controlled for using the Benjamini-Hochberg method (*80*).

Supplementary Materials

This PDF file includes:

Supplementary Text
Figs. S1 to S18
Tables S1 to S3

REFERENCES AND NOTES

1. Z. Huang, M. Skidmore, The impact of wildfires and wildfire-induced air pollution on house prices in the United States. *Land Econ.* **100**, 22–50 (2024).
2. M. Burke, A. Driscoll, S. Heft-Neal, J. Xue, J. Burney, M. Wara, The changing risk and burden of wildfire in the United States. *Proc. Natl. Acad. Sci. U.S.A.* **118**, e2011048118 (2021).
3. J. Bayham, J. K. Yoder, P. A. Champ, D. E. Calkin, The economics of wildfire in the United States. *Annu. Rev. Resour. Economics* **14**, 379–401 (2022).
4. D. Wang, D. Guan, S. Zhu, M. Mac Kinnon, G. Geng, Q. Zhang, H. Zheng, T. Lei, S. Shao, P. Gong, S. J. Davis, Economic footprint of California wildfires in 2018. *Nat. Sustain.* **4**, 252–260 (2020).
5. J. T. Abatzoglou, A. P. Williams, Impact of anthropogenic climate change on wildfire across western US forests. *Proc. Natl. Acad. Sci. U.S.A.* **113**, 11770–11775 (2016).
6. Y. Zhuang, R. Fu, B. D. Santer, R. E. Dickinson, A. Hall, Quantifying contributions of natural variability and anthropogenic forcings on increased fire weather risk over the western United States. *Proc. Natl. Acad. Sci. U.S.A.* **118**, e2111875118 (2021).
7. A. D. Syphard, S. J. E. Velazco, M. B. Rose, J. Franklin, H. M. Regan, The importance of geography in forecasting future fire patterns under climate change. *Proc. Natl. Acad. Sci. U.S.A.* **121**, e2310076121 (2024).
8. J. T. Abatzoglou, D. S. Battisti, A. P. Williams, W. D. Hansen, B. J. Harvey, C. A. Kolden, Projected increases in western US forest fire despite growing fuel constraints. *Commun. Earth Environ.* **2**, 227 (2021).
9. P. T. Brown, H. Hanley, A. Mahesh, C. Reed, S. J. Strenfel, S. J. Davis, A. K. Kochanski, C. B. Clements, Climate warming increases extreme daily wildfire growth risk in California. *Nature* **621**, 760–766 (2023).

10. A. P. Williams, J. T. Abatzoglou, A. Gershunov, J. Guzman-Morales, D. A. Bishop, J. K. Balch, D. P. Lettenmaier, Observed impacts of anthropogenic climate change on wildfire in California. *Earths Future* **7**, 892–910 (2019).
11. D. M. J. S. Bowman, C. A. Kolden, J. T. Abatzoglou, F. H. Johnston, G. R. van der Werf, M. Flannigan, Vegetation fires in the anthropocene. *Nat. Rev. Earth Environ.* **1**, 500–515 (2020).
12. M. A. Krawchuk, M. A. Moritz, Burning issues: Statistical analyses of global fire data to inform assessments of environmental change. *Environmetrics* **25**, 472–481 (2014).
13. National Interagency Coordination Center, Outlooks (NICC, 2023); www.nifc.gov/nicc/predictive-services/outlooks.
14. A. L. R. Westerling, Increasing western US forest wildfire activity: Sensitivity to changes in the timing of spring. *Philos. Trans. R. Soc. Lond. B. Biol. Sci.* **371**, 20150178 (2016).
15. W. M. Jolly, M. A. Cochrane, P. H. Freeborn, Z. A. Holden, T. J. Brown, G. J. Williamson, D. M. J. S. Bowman, Climate-induced variations in global wildfire danger from 1979 to 2013. *Nat. Commun.* **6**, 7537 (2015).
16. S. Strydom, M. J. Savage, Potential impacts of climate change on wildfire dynamics in the midlands of KwaZulu-Natal, South Africa. *Clim. Change* **143**, 385–397 (2017).
17. B. M. Wotton, M. D. Flannigan, Length of the fire season in a changing climate. *For. Chron.* **69**, 187–192 (1993).
18. J. T. Abatzoglou, C. A. Kolden, Climate change in Western US deserts: Potential for increased wildfire and invasive annual grasses. *Rangel. Ecol. Manage.* **64**, 471–478 (2011).
19. C. M. Countryman, *The Fire Environment Concept* (Pacific Southwest Forest and Range Experiment Station, 1972).
20. S. F. Arno, "Fire in Western Forest Ecosystems" in *Wildland Fire in Ecosystems: Effects of Fire on Flora*, J. K. Brown, J. K. Smith, Eds. (USDA Forest Service, 2000) vol. RMRS-GTR-42-vol 2, pp. 97–120.
21. J. W. van Wagtendonk, N. G. Sugihara, S. L. Stephens, A. E. Thode, K. E. Shaffer, J. A. Fites-Kaufman, Eds., *Fire in California's Ecosystems* (University of California Press, ed. 2, 2018).
22. G. J. Williamson, L. D. Prior, W. M. Jolly, M. A. Cochrane, B. P. Murphy, D. M. J. S. Bowman, Measurement of inter- and intra-annual variability of landscape fire activity at a continental scale: the Australian case. *Environ. Res. Lett.* **11**, 035003 (2016).
23. A. L. Westerling, H. G. Hidalgo, D. R. Cayan, T. W. Swetnam, Warming and earlier spring increase Western U.S. forest wildfire activity. *Science* **313**, 940–943 (2006).
24. P. E. Dennison, S. C. Brewer, J. D. Arnold, M. A. Moritz, Large wildfire trends in the western United States, 1984–2011. *Geophys. Res. Lett.* **41**, 2928–2933 (2014).
25. K. C. Short, Spatial wildfire occurrence data for the United States, 1992–2020 [FPA_FOD_20221014], 6th edition, Forest Service Research Data Archive (2022). https://doi.org/10.2737/RDS-2013-0009.6.
26. J. M. Omernik, G. E. Griffith, Ecoregions of the conterminous United States: Evolution of a hierarchical spatial framework. *Environ. Manag.* **54**, 1249–1266 (2014).
27. C. C. Hanes, X. Wang, P. Jain, M. A. Parisien, J. M. Little, M. D. Flannigan, Fire-regime changes in Canada over the last half century. *Can. J. For. Res.* **49**, 256–269 (2019).
28. R. C. Bales, N. P. Molotch, T. H. Painter, M. D. Dettinger, R. Rice, J. Dozier, Mountain hydrology of the western United States. *Water Resour. Res.* **42**, W08432 (2006).
29. Y. Jin, M. L. Goulden, N. Faivre, S. Veraverbeke, F. Sun, A. Hall, M. S. Hand, S. Hook, J. T. Randerson, Identification of two distinct fire regimes in Southern California: Implications for economic impact and future change. *Environ. Res. Lett.* **10**, 094005 (2015).
30. S. M. Byrne, M. A. Merrifield, M. L. Carter, D. R. Cayan, R. E. Flick, A. Gershunov, S. N. Giddings, Southern California winter precipitation variability reflected in 100-year ocean salinity record. *Commun. Earth Environ.* **4**, 143 (2023).
31. G. F. S. Boisramé, T. J. Brown, D. M. Bachelet, Trends in western USA fire fuels using historical data and modeling. *Fire Ecol.* **18**, 8 (2022).
32. J. K. Balch, B. A. Bradley, J. T. Abatzoglou, R. Chelsea Nagy, E. J. Fusco, A. L. Mahood, Human-started wildfires expand the fire niche across the United States. *Proc. Natl. Acad. Sci. U.S.A.* **114**, 2946–2951 (2017).
33. A. D. Syphard, J. E. Keeley, A. H. Pfaff, K. Ferschweiler, Human presence diminishes the importance of climate in driving fire activity across the United States. *Proc. Natl. Acad. Sci. U.S.A.* **114**, 13750–13755 (2017).
34. D. J. Parsons, S. H. DeBenedetti, Impact of fire suppression on a mixed-conifer forest. *For. Ecol. Manage.* **2**, 21–33 (1979).
35. C. C. Reed, S. M. Hood, D. R. Cluck, S. L. Smith, Fuels change quickly after California drought and bark beetle outbreaks with implications for potential fire behavior and emissions. *Fire Ecol.* **19**, 16 (2023).
36. J. W. van Wagtendonk, D. R. Cayan, Temporal and spatial distribution of lightning strikes in California in relation to large-scale weather patterns. *Fire Ecol.* **4**, 34–56 (2008).
37. J. E. Keeley, A. D. Syphard, Historical patterns of wildfire ignition sources in California ecosystems. *Int. J. Wildland Fire* **27**, 781–799 (2018).
38. B. Chen, Y. Jin, Spatial patterns and drivers for wildfire ignitions in California. *Environ. Res. Lett.* **17**, 055004 (2022).
39. P. E. Dennison, D. A. Roberts, S. H. Peterson, J. Rechel, Use of Normalized Difference Water Index for monitoring live fuel moisture. *Int. J. Remote Sens.* **26**, 1035–1042 (2005).
40. P. G. Brodrick, L. D. L. Anderegg, G. P. Asner, Forest drought resistance at large geographic scales. *Geophys. Res. Lett.* **46**, 2752–2760 (2019).
41. C. M. Countryman, W. A. Dean, "Measuring moisture content in living chaparral: A field user's manual" (Tech. Rep. PSW-36, US Department of Agriculture, Forest Service, Pacific Southwest Research Station, 1979).
42. M. Kretschmer, D. Coumou, J. F. Donges, J. Runge, Using causal effect networks to analyze different arctic drivers of midlatitude winter circulation. *J. Climate* **29**, 4069–4081 (2016).
43. J. Runge, P. Nowack, M. Kretschmer, S. Flaxman, D. Sejdinovic, Detecting and quantifying causal associations in large nonlinear time series datasets. *Sci. Adv.* **5**, eaau4996 (2019).
44. J. Runge, S. Bathiany, E. Bollt, G. Camps-Valls, D. Coumou, E. Deyle, C. Glymour, M. Kretschmer, M. D. Mahecha, J. Muñoz-Marí, E. H. van Nes, J. Peters, R. Quax, M. Reichstein, M. Scheffer, B. Schölkopf, P. Spirtes, G. Sugihara, J. Sun, K. Zhang, J. Zscheischler, Inferring causation from time series in Earth system sciences. *Nat. Commun.* **10**, 2553 (2019).
45. B. V. Smoliak, J. M. Wallace, P. Lin, Q. Fu, Dynamical adjustment of the Northern Hemisphere surface air temperature field: Methodology and application to observations. *J. Climate* **28**, 1613–1629 (2015).
46. B. Bass, J. Norris, C. Thackeray, A. Hall, Natural variability has concealed increases in western US flood hazard since the 1970s. *Geophys. Res. Lett.* **49**, e2021GL097706 (2022).
47. N. Siler, C. Proistosescu, S. Po-Chedley, Natural variability has slowed the decline in western U.S. snowpack since the 1980s. *Geophys. Res. Lett.* **46**, 346–355 (2019).
48. S. Sippel, N. Meinshausen, A. Merrifield, F. Lehner, A. G. Pendergrass, E. Fischer, R. Knutti, Uncovering the forced climate response from a single ensemble member using statistical learning. *J. Climate* **32**, 5677–5699 (2019).
49. J. Lund, J. Medellin-Azuara, J. Durand, K. Stone, Lessons from California's 2012–2016 drought. *J. Water Resour. Plan Manag.* **144**, 04018067 (2018).
50. R. Seager, M. Hoerling, S. Schubert, H. Wang, B. Lyon, A. Kumar, J. Nakamura, N. Henderson, Causes of the 2011–14 California drought. *J. Climate* **28**, 6997–7024 (2015).
51. A. L. Westerling, A. Gershunov, T. J. Brown, D. R. Cayan, M. D. Dettinger, Climate and wildfire in the western United States. *Bull. Am. Meteorol. Soc.* **84**, 595–604 (2003).
52. J. S. Littell, D. Mckenzie, D. L. Peterson, A. L. Westerling, Climate and wildfire area burned in western U.S. ecoprovinces, 1916–2003. *Ecol. Appl.* **19**, 1003–1021 (2009).
53. X. Huang, D. L. Swain, A. D. Hall, Future precipitation increase from very high resolution ensemble downscaling of extreme atmospheric river storms in California. *Sci. Adv.* **6**, eaba1323 (2020).
54. J. T. Abatzoglou, A. P. Williams, R. Barbero, Global emergence of anthropogenic climate change in fire weather indices. *Geophys. Res. Lett.* **46**, 326–336 (2019).
55. Z. A. Holden, A. Swanson, C. H. Luce, W. M. Jolly, M. Maneta, J. W. Oyler, D. A. Warren, R. Parsons, D. Affleck, Decreasing fire season precipitation increased recent western US forest wildfire activity. *Proc. Natl. Acad. Sci. U.S.A.* **115**, E8349–E8357 (2018).
56. M. L. Goulden, R. C. Bales, California forest die-off linked to multi-year deep soil drying in 2012–2015 drought. *Nat. Geosci.* **12**, 632–637 (2019).
57. USGCRP, *Fifth National Climate Assessment* (U.S. Global Change Research Program, Washington, DC, USA, 2023).
58. M. D. Dettinger, F. M. Ralph, T. Das, P. J. Neiman, D. R. Cayan, Atmospheric rivers, floods and the water resources of California. *Water* **3**, 445–478 (2011).
59. B. Langenbrunner, J. D. Neelin, Pareto-optimal estimates of California precipitation change. *Geophys. Res. Lett.* **44**, 12,436–12,446 (2017).
60. K. A. McKinnon, C. Deser, The inherent uncertainty of precipitation variability, trends, and extremes due to internal variability, with implications for western U.S. water resources. *J. Climate* **34**, 9605–9622 (2021).
61. D. L. Swain, A shorter, sharper rainy season amplifies California wildfire risk. *Geophys. Res. Lett.* **48**, e2021GL092843 (2021).
62. A. Gershunov, T. Shulgina, R. E. S. Clemesha, K. Guirguis, D. W. Pierce, M. D. Dettinger, D. A. Lavers, D. R. Cayan, S. D. Polade, J. Kalansky, F. M. Ralph, Precipitation regime change in Western North America: The role of Atmospheric Rivers. *Sci. Rep.* **9**, 9944 (2019).
63. D. R. Gergel, B. Nijssen, J. T. Abatzoglou, D. P. Lettenmaier, M. R. Stumbaugh, Effects of climate change on snowpack and fire potential in the western USA. *Clim. Change* **141**, 287–299 (2017).
64. M. J. Koontz, M. P. North, C. M. Werner, S. E. Fick, A. M. Latimer, Local forest structure variability increases resilience to wildfire in dry western U.S. coniferous forests. *Ecol. Lett.* **23**, 483–494 (2020).
65. K. Rao, A. P. Williams, N. S. Diffenbaugh, M. Yebra, C. Bryant, A. G. Konings, Dry live fuels increase the likelihood of lightning-caused fires. *Geophys. Res. Lett.* **50**, e2022GL100975 (2023).
66. J. T. Abatzoglou, C. A. Kolden, J. K. Balch, B. A. Bradley, Controls on interannual variability in lightning-caused fire activity in the western US. *Environ. Res. Lett.* **11**, 045005 (2016).
67. J. T. Abatzoglou, S. Z. Dobrowski, S. A. Parks, K. C. Hegewisch, TerraClimate, a high-resolution global dataset of monthly climate and climatic water balance from 1958–2015. *Sci. Data* **5**, 170191 (2018).
68. H. Hersbach, B. Bell, P. Berrisford, G. Biavati, A. Horányi, J. Muñoz Sabater, J. Nicolas, C. Peubey, R. Radu, I. Rozum, D. Schepers, A. Simmons, C. Soci, D. Dee, J.-N. Thépaut, ERA5

monthly averaged data on single levels from 1940 to present. Copernicus Climate Change Service (C3S) Climate Data Store (CDS) (2023); https://doi.org/10.24381/cds.f17050d7.
69. P. G. Brodrick, L. D. L. Anderegg, G. P. Asner, Dry-season canopy water content maps for California vegetation from 1990–2017, link to GeoTiffs, PANGAEA (2019); https://doi.pangaea.de/10.1594/PANGAEA.897276.
70. L. E. Flint, A. L. Flint, J. H. Thorne, R. Boynton, Fine-scale hydrologic modeling for regional landscape applications: The California Basin Characterization Model development and performance. *Ecol. Process.* **2**, 25 (2013).
71. U.S. Geological Survey, Annual National Land Cover Database (NLCD) Collection 1 Products, www.usgs.gov/data/annual-national-land-cover-database-nlcd-collection-1-products.
72. P. Spirtes, C. Glymour, An algorithm for fast recovery of sparse causal graphs. *Soc. Sci. Comput. Rev.* **9**, 62–72 (1991).
73. D. S. Wilks, Resampling hypothesis tests for autocorrelated fields. *J. Climate* **10**, 65–82 (1997).
74. Y. Pourmohamad, J. T. Abatzoglou, E. J. Belval, E. Fleishman, K. Short, M. C. Reeves, N. Nauslar, P. E. Higuera, E. Henderson, S. Ball, A. Aghakouchak, J. P. Prestemon, J. Olszewski, M. Sadegh, Physical, social, and biological attributes for improved understanding and prediction of wildfires: FPA FOD-Attributes dataset. *Earth Syst. Sci. Data* **16**, 3045–3060 (2024).
75. C. Deser, F. Lehner, K. B. Rodgers, T. Ault, T. L. Delworth, P. N. DiNezio, A. Fiore, C. Frankignoul, J. C. Fyfe, D. E. Horton, J. E. Kay, R. Knutti, N. S. Lovenduski, J. Marotzke, K. A. McKinnon, S. Minobe, J. Randerson, J. A. Screen, I. R. Simpson, M. Ting, Insights from Earth system model initial-condition large ensembles and future prospects. *Nat. Clim. Change* **10**, 277–286 (2020).
76. P. K. Sen, Estimates of the regression coefficient based on Kendall's tau. *J. Am. Stat. Assoc.* **63**, 1379–1389 (1968).
77. H. Theil, "A rank-invariant method of linear and polynomial regression analysis," in *Henri Theil's Contributions to Economics and Econometrics: Econometric Theory and Methodology*, (Springer, 1992), pp. 345–381.
78. H. B. Mann, Nonparametric tests against trend. *Econometrica* **13**, 245–259 (1945).
79. M. G. Kendall, Rank and product-moment correlation. *Biometrika* **36**, 177–193 (1949).
80. Y. Benjamini, Y. Hochberg, Controlling the false discovery rate: A practical and powerful approach to multiple testing. *J. R. Stat. Soc. Ser. B. Stat. Methodol.* **57**, 289–300 (1995).

Acknowledgments: We acknowledge computing support from the Casper system (https://ncar.pub/casper) provided by the NSF National Center for Atmospheric Research (NCAR), sponsored by the National Science Foundation. We acknowledge support from the Sustainable LA Grand Challenges program at UCLA. **Funding:** This research was funded by the University of California Laboratory Fees Research Program (LFR-18-542511); the Department of Energy, Office of Science HyperFACETS project (DE-SC0016605); the Gordon and Betty Moore Foundation (grant 11974); and the USGS Southwest Climate Adaptation Science Center (USGS 314653-00001 and G24AC00611). **Author contributions:** Conceptualization: G.D.M., M.A.M., A.P.W., and A.H. Methodology: G.D.M., M.A.M., A.P.W., K.A.M., R.F., A.H., and S.R. Software: G.D.M. and M.A.M. Validation: G.D.M. and M.A.M. Formal analysis: G.D.M. Investigation: G.D.M., M.A.M. Resources: G.D.M., M.A.M., and S.R. Data curation: G.D.M., M.A.M., S.R., and B.B. Writing—original draft: G.D.M. Writing—review and editing: G.D.M., M.A.M., A.P.W., K.A.M., R.F., A.H., and J.N. Visualization: G.D.M. and M.A.M. Supervision: G.D.M., M.A.M., A.P.W., A.H., and K.A.M. Project administration: G.D.M., A.H., and M.A.M. Funding acquisition: A.H., M.A.M., A.P.W., B.B., and G.D.M. **Competing interests:** The authors declare that they have no competing interests. **Data and materials availability:** All data needed to evaluate the conclusions in the paper are present in the paper and/or the Supplementary Materials. Data used in the study are available from the links below. FPA-FOD fire occurrence data: www.fs.usda.gov/rds/archive/catalog/RDS-2013-0009.6; TerraClimate: www.climatologylab.org/terraclimate.html; canopy water content: https://doi.org/10.1594/PANGAEA.897276; LFMC: https://fems.fs2c.usda.gov; ERA5: https://doi.org/10.24381/cds.f17050d7; and NLCD: https://doi.org/10.5066/P94UXNTS. LFMC data obtained from the US National Fuel Moisture Database for California are available at https://doi.org/10.5281/zenodo.15627740.

Submitted 17 September 2024
Accepted 8 July 2025
Published 6 August 2025
10.1126/sciadv.adt2041